OXFORD

SOT | Society of Toxicology
www.toxsci.oxfordjournals.org

*TOXICOLOGICAL SCIENCES*, 154(1), 2016, 27–42

doi: 10.1093/toxsci/kfw155
Advance Access Publication Date: August 10, 2016
Research article

# Ethylmercury-Induced Oxidative and Endoplasmic Reticulum Stress-Mediated Autophagic Cell Death: Involvement of Autophagosome–Lysosome Fusion Arrest

Ji-Yoon Choi*, Nam-Hee Won†, Jung-Duck Park‡, Sinae Jang§, Chi-Yong Eom§, Yongseok Choi*, Young In Park¶,[1], and Mi-Sook Dong*,[2]

*School of Life Sciences and Biotechnology, Korea University, Seoul, Korea; †College of Medicine, Korea University, Seoul, Korea; ‡College of Medicine, Chung-Ang University, Seoul, Korea; §Seoul Center, Korea Basic Science Institute, Seoul, Korea; and ¶College of Pharmacy, Korea University, Sejong, Korea

[1]To whom Co-Correspondence should be addressed. Fax: +82-41-860-1606. E-mail: yipark@korea.ac.kr.
[2]To whom Correspondence should be addressed. Fax: 82 2 3290 3951. E-mail: msdong@korea.ac.kr.



## ABSTRACT

Ethylmercury (EtHg) is derived from the degradation of thimerosal, the most widely used organomercury compound. In this study, EtHg-induced toxicity and autophagy in the mouse kidney was observed and then the mechanism of toxicity was explored *in vitro* in HK-2 cells. Low doses of EtHg induced autophagy without causing any histopathological changes in mouse kidneys. However, mice treated with high doses of EtHg exhibited severe focal tubular cell necrosis of the proximal tubules with autophagy. EtHg dose-dependently increased the production of reactive oxygen species, reduced the mitochondrial membrane potential, activated the unfolded protein response, and increased cytosolic $Ca^{2+}$ levels in HK-2 cells. Cell death induced by EtHg exposure was caused by autophagy and necrosis. *N*-acetyl cysteine and 4-phenylbutyric acid attenuated EtHg-induced stress and ameliorated the autophagic response in HK-2 cells. Furthermore, EtHg blocked autophagosome fusion with lysosomes, which was demonstrated via treatment with wortmannin and chloroquine. Low doses of EtHg and rapamycin, which resulted in minimal cytotoxicity, increased the levels of the autophagic SNARE complex STX17 (syntaxin 17)-VAMP8-SNAP29 without altering mRNA levels, but high dose of EtHg was cytotoxic. Inhibition of autophagic flux by chloroquin increased autophagosome formation and necrotic cell death in HK-2 cells. Collectively, our results show that EtHg induces autophagy via oxidative and ER stress and blockade of autophagic flux. Autophagy might play a dual role in EtHg-induced renal toxicity, being both protective following treatment with low doses of EtHg and detrimental following treatment with high doses.

**Key words:** ethylmercury; ER stress; mitochondrial dysfunction; autophagy; blocking autophagic flux

Mercury is a serious environmental pollutant worldwide; it is produced by industrial processes. It is unique among the heavy metals found in the environment because it takes several physical and chemical forms: elemental mercury, inorganic mercury, and organic mercury (Zalups, 2000). Although the distribution, toxicity, and metabolism of mercury are highly dependent on its chemical form, the primary toxic targets of inorganic and organic mercury compounds are the kidneys and central nervous system, respectively, in humans and animals (Clarkson and Magos, 2006). Methylmercury (MeHg) and ethylmercury (EtHg) are short-chain alkyl mercurial compounds with similar chemical properties. MeHg is known to be one of the most toxic forms of Hg and the most common form of mercury exposure in fish-eating populations. EtHg is derived from the metabolism of

thimerosal (O-carboxyphenyl-thio-ethyl-sodium salt), a form of organic mercury widely used as a vaccine preservative. The *in vitro* toxicity of EtHg and thimerosal is comparable to the toxicity of MeHg (Dorea *et al.*, 2013). However, in the body, EtHg differs from MeHg in that it is more rapidly converted to inorganic mercury, which results in kidney damage (Clarkson and Magos, 2006).

The renal toxicity of mercury is related to both its accumulation in the proximal tubules and its intracellular binding to thiol groups, which are important constituents of enzymes, transcription factors, and several cellular components. This strong reactivity with various molecules is reflected by the capacity of Hg to disturb a variety of cellular and biochemical processes. The inactivation of thiol-rich molecules by mercury significantly increases the production of reactive oxygen species (ROS) (Lu *et al.*, 2010). The oxidative stress involved in mercury-induced cellular toxicity destroys homeostasis in pro-oxidant and antioxidant fashions (Grotto *et al.*, 2010).

The endoplasmic reticulum (ER) is an important organelle responsible for several normal cellular functions, including synthesis, folding, and modification of proteins; lipid synthesis; and $Ca^{2+}$ storage. When chaperone-assisted protein folding in the ER is impaired by certain physiological and pathological conditions, ER stress occurs. ER stress causes unfolded and misfolded proteins to be retained in the ER, which activates a signaling response termed the unfolded protein response (UPR) (Wu and Kaufman, 2006). The UPR stress sensors inositol-requiring protein 1α (IRE1α), protein kinase RNA-like endoplasmic reticulum kinase (PERK), and activating transcription factor 6 (ATF6) transduce information about the protein folding status within the ER to the cytosol and nucleus in an effort to restore protein-folding capacity. Mild or moderate ER stress results in critical adaptation phenotypes, inhibition of protein synthesis, ER-associated degradation, and other responses that lessen protein folding in the ER. Severe ER stress causes cell death (Tabas and Ron, 2011).

Chemical toxicity is associated with multiple modes of cell death, including apoptosis, autophagy, and necrosis. The mode of cell death triggered by certain toxicants depends on the dose. Exposure to toxicants at low doses most often results in autophagy or apoptosis, whereas higher levels of the same toxicant might cause necrosis (Marino *et al.*, 2014). Autophagy has been recognized as an essential part of cellular homeostasis and the activation of autophagy can protect cells from various insults. However, autophagy can be thought of as a double-edged sword in the pathogenesis of many human diseases. It has been shown to perform a protective role in many instances, but has also been found to contribute to cell death under different circumstances (Decuypere *et al.*, 2015; Zhang *et al.*, 2016). Autophagy involves a highly ordered pathway which begins with the formation of a double-membrane vesicle, termed an 'autophagosome.' Formation of the autophagosome membrane and subsequent fusion with a lysosome requires the sequential recruitment of various proteins involved in vesicle (phagopore) nucleation, elongation, and fusion to form complexes called autophagolysosomes or autolysosomes, which allow for degradation of the contents of the autophagosome by lysosomal hydrolytic enzymes. The conversion of microtubule-associated protein 1 light chain 3 (LC3-I) to LC3-II, which is accomplished by the association of its phosphatidylethanolamine-conjugated moiety with the autophagosome membrane, is the main molecular marker for the formation of early autophagosomes (Kuma *et al.*, 2004). Autophagosome fusion with a lysosome constitutes the last barrier for autophagic degradation. It is thought that this fusion process is precisely and tightly regulated. Recent genetic evidence suggests that autophagic SNARE (soluble N-ethylmaleimide-sensitive fusion attachment protein receptors) complexes, including STX17, SNAP29, and VAMP8, are essential for the fusion of autophagosomes and lysosomes (Amaya *et al.*, 2015; Itakura *et al.*, 2012; Zhen and Li, 2015).

Recent reports have demonstrated the induction of autophagy following Hg exposure in neuronal stem cells and liver cells (Chang *et al.*, 2013; Chatterjee *et al.*, 2014a; Zhang *et al.*, 2014). Although all forms of mercury are potent disruptors of cellular functions, targeting a variety of cellular regulatory pathways that are capable of inflicting various degrees of cellular damage via multiple mechanisms, the molecular mechanism of EtHg-induced renal proximal tubular cell toxicity remains poorly understood, particularly in autophagy-related cell death. In this study, we investigated the roles of mitochondrial dysfunction and endoplasmic reticulum (ER) stress on EtHg-induced cytotoxicity, particularly autophagy, in HK-2 cells and in an *in vivo* mouse model.

## MATERIALS AND METHODS

*Materials*. All mercury chemicals were obtained from Alfa Aesar (A Johnson Matthey Company, Ward Hill, Massachusetts). Antibodies specific for eIF2α, phospho-eIF2α, CHOP, Grp78, XBP1, Caspase-2, -3, -8, -9, -12, PARP, LC3B, Beclin 1, p62, Cathepsin B, LAMP1, HMGB1, STX17, SNAP29, and VAMP8 were purchased from Cell Signaling Technologies (Beverly, Massachusetts), and the antibody against β-actin was obtained from Santa Cruz Biotechnology (Santa Cruz, California).

*In vivo study*. Animal studies were conducted in accordance with the institutional guidelines for the care and use of laboratory animals, and the experimental protocol was approved by the Animal Ethics Committee of Korea University (approval number: KUIACUC-2012-94). Five-week-old specific pathogen-free C57BL/6 mice were obtained from Orient Bio Inc. (Gapyung, Korea) and caged in an animal room maintained at $22 \pm 2\,^{\circ}C$ with a 12-h light/dark cycle and a relative humidity of 40–50%. The animals had free access to tap water and a pellet diet (Jeiljedang, Seoul, Korea). After a 7-day acclimation period, the mice were weighed and randomly divided into 5 experimental groups ($n = 6$). Because the major administration rout of EtHg is injection of the thimerosal form, mice were administered saline or EtHg by intraperitoneal injection. Group 1 was the vehicle control (10 ml/kg body weight (bw)/day saline), and groups 2, 3, 4, and 5 were treated with 1, 2, 5, and 10 mg EtHg/10 ml/kg bw/day, respectively, in saline for 3 consecutive days. Eight hours after the last treatment, the mice were anaesthetized with ethyl ether and blood was collected from the abdominal aorta. The kidneys were removed, weighed, and fixed in a 10% formalin solution containing PBS until histological examination. Blood was centrifuged at $1500 \times g$ for 20 min at $4\,^{\circ}C$ to prepare plasma. CRE and BUN were analyzed using a biochemical blood analyzer (Hitachi 7180, Hitachi, Japan). Animals were observed at least once each day during the experimental period. Body weights and any abnormalities were recorded daily.

*Histopathological evaluation*. For routine histopathologic examination, bisected kidneys were fixed in 10% neutral formalin and embedded in paraffin. Each 4-μm-thick section was stained with hematoxylin and eosin (H&E) and periodic acid Schiff (PAS), and the extent of damage was evaluated using light microscopy.

*Analysis of ethylmercury in tissue*. The total concentration of EtHg in kidney tissue was determined with a Direct Mercury

Analyzer-80 (DMA-80, Milestone, Italy) using the gold-amalgam method. Briefly, 100 mg of kidney tissue was placed into a nickel boat and processed through 3 stages (drying, ashing, and atomizing). The concentration of mercury in kidney tissue was calculated from a standard calibration curve produced using a standard EtHg solution (1000 ppm, Aldrich, St. Louis, Missouri). The concentration of mercury in kidney tissue was expressed as μg/g wet weight. A standard reference material (SRM, Bio-Rad, Irvine, California) was used for validation.

*Cell line and culture conditions*. All assays were performed using human and rat renal proximal tubular cell lines, HK-2 and NRK-52E, respectively. HK-2 (human kidney 2) cells are proximal tubular cells derived from normal kidneys and were obtained from the American Type Culture Collection (ATCC; Manassas, Virginia) and grown in Keratinocyte Serum Free Media (K-SFM) containing bovine pituitary extract (BPE) and human recombinant epidermal growth factor (EGF), which were supplied with each of the 2 additives required for growth of this cell line (Invitrogen, Grand Island, New York). NRK-52E, a rat renal proximal tubular cell line, was obtained from ATCC and cultured in Dulbecco's Modified Eagle's Medium supplemented with 5% fetal bovine serum. The cells were maintained at 37 °C in a humidified 5% $CO_2$ atmosphere. For the inhibition study, 5 mM N-acetyl cysteine (NAC) as an L-cysteine precursor, the antioxidant trolox (100 μM), and 2 mM 4-phenyl butyric acid (4-PBA) as a chemical chaperone were used to pre-treat the cells for 2 h.

*Cell proliferation and cytotoxicity assays*. Cell proliferation was determined using the CellTiter 96 Non-Radioactive Cell Proliferation Assay kit according to the manufacturer's protocol (Promega, Madison, Wisconsin). HK-2 cells were seeded in 96-well plates at a density of $5 \times 10^3$ cells/well. The following day, organic mercury compounds were added and the cells were incubated for 24 h. To determine the time- and dose-dependent cytotoxicity of EtHg, varying concentrations of EtHg were added to the wells and cells were incubated for 6, 12, 24, and 48 h. After adding MTS (3-(4,5-dimethylthiazol-2-yl)-5-(3-carboxymethoxyphenyl)-2-(4-sulfophenyl)-2H-tetrazolium) solution, the plates were incubated at 37 °C in a $CO_2$ incubator for 3 h, and absorbance was measured at 490 nm using a microplate reader (Bio-Rad, California).

*Quantitative measurement of reactive oxygen species (ROS)*. The intracellular ROS level was quantitatively analyzed using the fluorescent dye carboxy-$H_2$DCFDA (Molecular Probes, Eugene, Oregon). Flow cytometric (FACS) analysis (BD, Fullerton, California) was performed to determine ROS generation in EtHg-treated cells. HK-2 cells were exposed to 0.1-2 μM EtHg for 3 h and then stained with 5 mM carboxy-$H_2$DCFDA (5-6-carboxy-2′,7′-dichlorodihydrofluorescein diacetate) for 30 min, washed with phosphate-buffered saline (PBS), and placed in the dark. As a positive control, HK-2 cells were treated with 500 μM $H_2O_2$ for 3 h and analyzed by flow cytometry with a FACScan using the CELLQuest program (BD, Fullerton, California).

*Assessment of mitochondrial membrane potential*. The fluorescent probe JC-1 (Molecular Probes, Eugene, OR) and the Mitoprobe™ $DiOC_2(3)$ assay kit (Invitrogen, Grand Island, New York) were used to estimate $\Delta\psi_m$ (MMP). HK-2 cells were adjusted to a density of $2 \times 10^5$ cells/well in a 48-well plate, and cells were treated with 500 μM $H_2O_2$, 1 μg/ml valinomycin (a positive control which renders the mitochondrial membrane permeable to $K^+$ ions), or various concentrations of EtHg for 24 h. The cells were stained with 100 μl of JC-1 at 37 °C for 20 min and then washed 3 times with PBS. The results were observed through a fluorescence microscope (Nikon Co., Tokyo, Japan). Aggregates and monomers were visualized in the mitochondria using G-2A and B-2A filters, respectively, and quantitated with the NIS-Elements BR program (Nikon Co., Tokyo, Japan). The Mitoprobe™ $DiOC_2(3)$ assay kit for flow cytometry with a FACScan system using the CELLQuest program (BD, Fullerton, California) were used as described by the manufacturer. Briefly, HK-2 cells were adjusted to a density of $2 \times 10^5$ cells/well in a 48-well plate, and cells were treated with 500 μM $H_2O_2$ or various concentrations of EtHg for 24 h. Cells were then suspended in 1 ml of PBS, loaded with 5 μl of 10 μM $DiOC_2(3)$, and incubated at 37 °C for 20min. For a positive control, cells were treated with 1 μl of 50 mM carbonyl cyanide m-chlorophenylhydrazone (CCCP) and incubated at 37 °C for 5 min. Cells were washed with PBS and analyzed immediately using flow cytometry at an excitation wavelength of 488 nm and an emission wavelength of 525 nm.

*Measurement of intracellular $Ca^{2+}$ concentration*. $[Ca^{2+}]_i$ was measured using a previously described procedure (Zaitsu *et al.*, 2007). HK-2 cells were seeded in 24-well culture plates at $2 \times 10^4$ cells/well and allowed to attach to the plates for 24 h. The cells were rinsed twice with HEPES buffer (pH 7.4; 10 mM HEPES, 140 mM NaCl, 5 mM KCl, 1 mM $CaCl_2$) and treated with flou-3AM (5 μM) in HEPES buffer for 30 min at 37 °C. The cells were then washed with HEPES buffer to remove free flou-3AM. Experimental cells were exposed to EtHg for 8 min and monitored with a laser scanning microscope (LSM 510 META, Carl Zeiss, Germany).

*RT-PCR and real time-quantitative (RT-qPCR) analysis*. After HK-2 cells were treated with tunicamycin (TM) or EtHg for 6 h, total cellular RNA was isolated using the easy-BLUE™ Total RNA Extraction Kit (iNtRON, Korea) according to the manufacturer's instructions. All PCR primers were synthesized using published sequences or sequences found in the NCBI nucleotide sequence database, and are listed in Table S1. The amplification reactions were performed in a MyiQ thermal cycler (Bio-Rad, California). Relative mRNA levels were quantified by normalization to the housekeeping gene β-actin. RT-qPCR was performed in triplicate using the KAPA SYBR FAST qPCR kit (Applied Kapabiosystems) in a MyiQ thermal cycler under the following conditions: 95 °C for 3 min, followed by 40 cycles at 95 °C for 30 s and 60 °C for 30 s. β-actin was amplified in parallel as an internal control for each run. The fluorescence cycle thresholds (Ct) were obtained using iCycler software version 2.0 (Bio-Rad) and were averaged (SD ≤ 1). Gene expression was normalized to the reference gene, and relative expression levels were calculated as previously described (Kroemer and Reed 2000).

*Detection of apoptotic cells*. HK-2 cells were treated with EtHg for 24 h, washed twice with cold PBS, and incubated with Annexin V-FITC (BD, Fullerton, Calfornia) for 15 min at room temperature in the dark. Apoptosis was analyzed by flow cytometry with a FACScan using the CELLQuest program (BD, Fullerton, California).

*Immunoblot analysis*. After removal of the medium, EtHg-treated HK-2 cells were washed 3 times with ice-cold PBS. Whole cell lysates were prepared in radioimmunoprecipitation assay (RIPA) buffer (iNtRON, Korea), incubated on ice for 10 min, and centrifuged at 18 000 × g for 30 min at 4 °C, and then protein content was quantified. Equal amounts of protein were separated by SDS-polyacrylamide gel electrophoresis on a 12% gel and then transferred to a polyvinylidene difluoride membrane. The membranes were immunoblotted with the corresponding primary antibodies and goat anti-mouse or anti-rabbit IgG-HRP secondary antibodies for 1 h and then developed with chemiluminescence reagents (Pierce, Rockford, Illinois) and examined using the LAS-3000 imaging system (Fujifilm, Tokyo, Japan).

*Establishment of the NRK52E/GFP_LC3 cell line and detection of GFP-LC3 puncta and fluorescent staining with lysotracker red.* pGFP-LC3 was kindly provided by Dr. Hye-Jin Lee (Hallym University, Chunchon, Korea). NRK-52E cells were transfected with pGFP-LC3 using Lipofectamine 2000 (Invitrogen, Carlsbad, California) according to the manufacturer's protocol. Clones stably expressing GFP-LC3 were selected with G148 antibiotics. An autofluorescent compound, LysoTracker® Red DND-99 (LysoTR, Invitrogen, Carlsbad, California), was used as a marker of lysosomes. Briefly, NRK-52E/GFP_LC3 cells were plated on coverslips and treated with EtHg for 24 h. Cells were stained with 400 ng/μL LysoTR at 37 °C and then washed with PBS. Images were taken using a Carl Zeiss LSM 510 META confocal microscope (Germany) and Leica TCS SP8 confocal microscope (Germany). The images were analyzed with Leica software (LAS X).

*Cell vitality assay*. HK-2 cells were incubated with or without EtHg for 24 h, trypsinized, washed with PBS, and suspended in solution 6 (VitaBright-48, PI). Cell viability was immediately analyzed using a NucleoCounter NC-250™ imaging cytometer (Chemometec, Denmark) according to the manufacturer's specifications.

*Statistical analysis*. All results are expressed as mean ± standard deviation (SD). The student's t-test was used for analysis of the *in vitro* experiments, and analysis of variance (ANOVA) was used to compare blood biochemistry between the 4 treated groups and the control animals. The histopathologic results were analyzed using Chi-square tests. The levels of significance were set at $P < .05$ and $P < .01$.

## RESULTS

### *Effect of Organic Mercury Compounds on the Viability of HK-2 Cells*

To select an *in vitro* nephrotoxic organic mercury compound, the cytotoxicity of a 5 μM dose of 5 organic mercury compounds [MBH, mercury (II) benzoate hydrate; DBM, dibenzylmercury; DPM, diphenylmercury (II); MeHg, methylmercury (II) iodide, and EtHg] were determined in HK-2 cells (Figure 1A). The compounds were cytotoxic in the following order: EtHg > MeHg > DBH > DPM > MBH. Therefore, EtHg was selected to explore the nephrotoxic mechanism of mercury in HK-2 cells. To define the profile of EtHg cytotoxicity, HK-2 cells were treated with EtHg at concentrations ranging from 0.25 to 4 μM for various exposure times between 6 and 48 h (Figure 1B). EtHg was cytotoxic to HK-2 cells in a dose- and time-dependent manner, with $IC_{50}$ values of 9.6, 9.5, 2.2 and 1.1 μM at 6, 12, 24, and 48 h, respectively.

### *EtHg Induces ER Stress and Autophagy in Mice*

Autophagy has been shown to be the initial response of a cell to a toxic metal in a concentration- and time-dependent manner (Chatterjee *et al.*, 2014a). However, the occurrence of autophagy following Hg exposure was previously investigated in neuronal stem cells and liver cells (Chang *et al.*, 2013; Zhang *et al.*, 2014), but not in kidney cells. Therefore, we studied EtHg-induced kidney toxicity via autophagy in mice. EtHg was administered to mice by intraperitoneal injection at doses of 0, 1, 2, 5, and 10 mg/kg bw/day for 3 consecutive days. Body weight and the biomarkers of kidney damage creatinine (CRE) and blood urea nitrogen (BUN) were not significantly different between most groups, except that they did differ between group 5 (10 mg/kg bw/day) and group 1 (control). However, the total mercury content in kidney tissue was significantly increased in a dose-dependent manner in all EtHg treatment groups (Table 1). Light microscopy indicated that the low-dose groups (groups 2 and 3) showed no changes compared with the normal control group (group 1). In group 4, focal tubular cell necrosis of proximal tubules was observed in the outer medullary area (Figure 2A, arrow). In the high-dose group (group 5), there was extensive tubular cell necrosis in the outer medulla. At a higher magnification insert, neutrophilic infiltrates around the necrotic tubular cells were observed (Figure 2A, arrowhead).

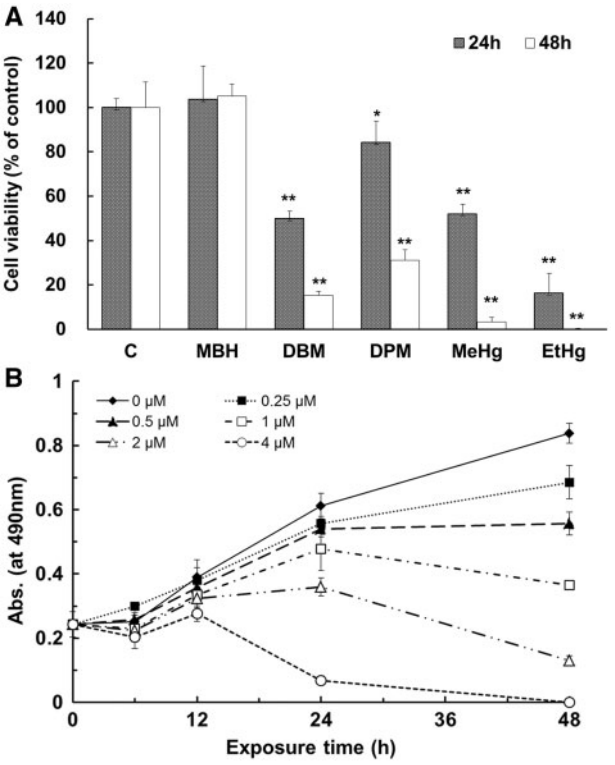


FIG. 1. Cytotoxicity of A, 5 organomercury compounds and B, ethylmercury in HK-2 cells. A, Effect of exposure to 5 organomercury compounds on the viability of HK-2 cells. HK-2 cells were exposed to 5 organomercury compounds at a concentration of 5 μM for 24 and 48 h. The values shown represent the means ± SD ($n = 3$). B, Dose- and time-dependent cytotoxic effects of EtHg. EtHg was applied at 0.25, 0.5, 1, 2, and 4 μM concentrations for 0, 6, 12, 24, and 48 h. The values shown represent means ± SD ($n = 6$). Cell viability was measured using the MTS assay as described in the Materials and Methods section. *$P < 0.05$, and **$P < 0.01$ compared with untreated controls.

To test whether EtHg can induce ER stress in mouse kidney tissue, Grp78, Xbp1, and Chop were evaluated at the mRNA and protein levels. The mRNA levels of those ER stress markers were not significantly altered in the low-dose groups (groups 2 and 3); however, in group 4, the mRNA levels of Grp78 and Chop were significantly increased, by approximately 1.4- and 2.6-fold, respectively, compared with group 1 (Figure 2B). In contrast to the mRNA levels, the protein levels of the ER stress-related markers were significantly altered in the low-dose groups (1 and 2 mg/kg bw/day groups), in which the mice did not show any biochemical or pathological changes in blood or kidney tissue (Figure 2C; Table 1). GRP78 protein levels were dramatically increased in groups 4 and 5, in which pathologic changes in kidney tissue were observed, and CHOP protein expression was induced at the highest level in group 3. The expression of the autophagy marker protein LC3B-II was maximally elevated, approximately 3.6-fold, in the low-dose groups compared with group 1. However, in the groups with kidney tissue damage (groups 4 and 5), the expression of this protein was only 2.6- and 3.2-fold higher, respectively, than in group 1 (Figure 2D).

**TABLE 1.** Physiological and Biochemical Characteristics of Mice Treated with Various Doses of Ethylmercury for 3 Consecutive Days

| | Group 1 (control) | Group 2 (1 mg/kg) | Group 3 (2 mg/kg) | Group 4 (5 mg/kg) | Group 5 (10 mg/kg) |
|---|---|---|---|---|---|
| Body weight (g) | | | | | |
| Day 1 | 22 ± 0.39 | 23 ± 0.91 | 23 ± 0.36 | 22 ± 0.40 | 22 ± 0.55 |
| Day 2 | 22 ± 0.33 | 21 ± 1.00 | 22 ± 0.44 | 21 ± 0.30 | 20 ± 0.80 |
| Day 3 | 23 ± 0.34 | 23 ± 1.13 | 23 ± 0.61 | 21 ± 0.71 | 19 ± 1.09 |
| CRE (mg/dl) | 0.23 ± 0.05 | 0.22 ± 0.04 | 0.20 ± 0.00 | 0.20 ± 0.00 | 1.17 ± 0.12* |
| BUN (mg/dl) | 14.6 ± 1.28 | 12.4 ± 1.68 | 19.5 ± 1.90 | 15.6 ± 7.27 | 210 ± 30.0* |
| Total mercury content (μg/g tissue) | 0.067 ± 0.018 | 28.5 ± 5.92* | 42.5 ± 7.36* | 66.9. ± 22.4* | 95.1 ± 14.0* |

*$P < 0.01$ compared with untreated controls.

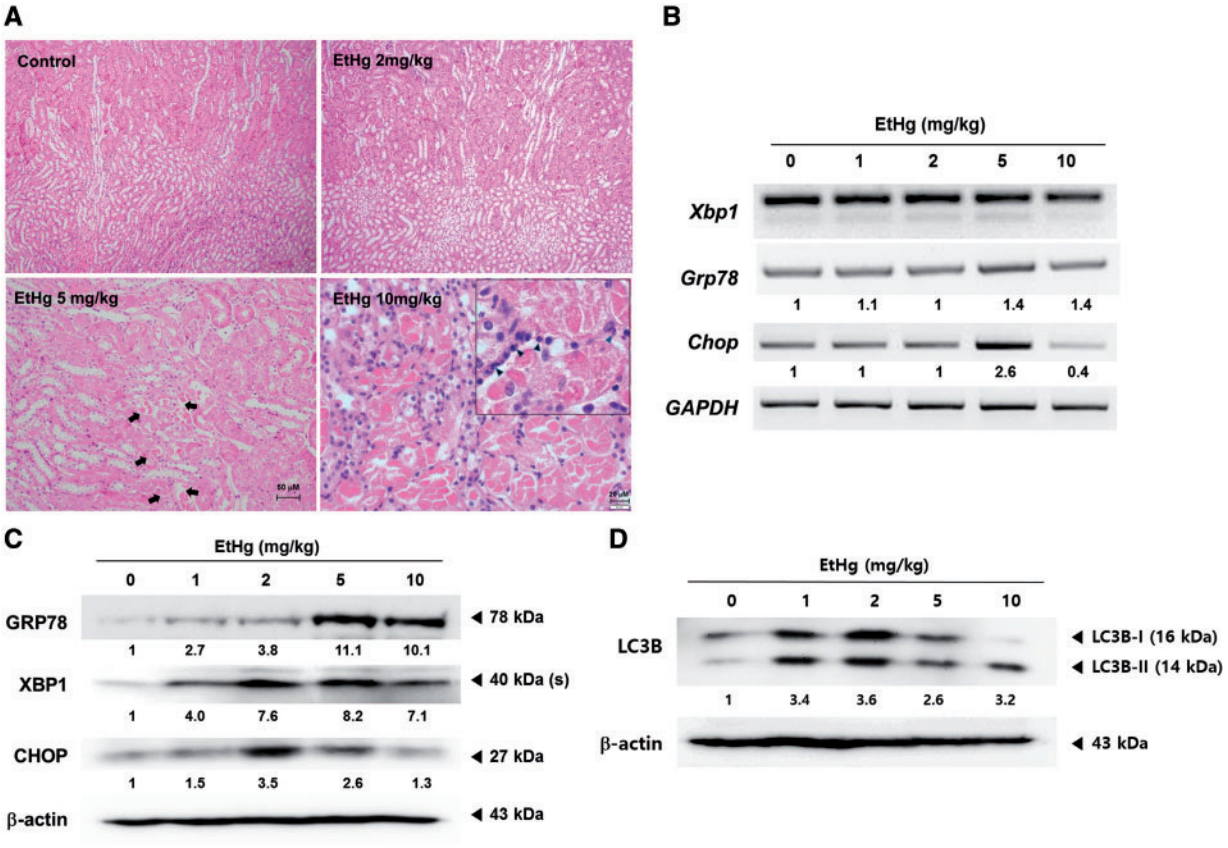


**FIG. 2.** EtHg induces ER stress and autophagy in the mouse kidney. A, Histological analysis of H&E-stained sections from mouse kidneys. B, The gene expression levels of ER stress markers (Xbp1, BiP, and CHOP) in kidney tissues were analyzed using RT-PCR. Representative ER stress-related protein levels (C) and LC3B conversion as an autophagy marker (D) were detected by immunoblotting. Six-week-old male mice were treated with saline (group 1) or 1, 2, 5, or 10 mg/kg/day EtHg (groups 2–5) by intraperitoneal injection for 3 consecutive days (control group, $n = 6$; other groups, $n = 5$).

These results indicate that subtoxic doses of EtHg can induce ER stress and autophagy.

### *EtHg Induces the Unfolded Protein Response (UPR) in a Dose- and Time-Dependent Manner*

EtHg-induced ER stress in mice was confirmed in HK-2 cells using a positive control, tunicamycin (TM), which is a commonly used ER stressor. Dose-dependent expression of the ER stress-related genes Chop, Grp78, and Erdj4 in EtHg-treated HK-2 cells was assessed by semi-quantitative RT-PCR (Supplementary Figure 1A). Splicing of Xbp1 mRNA was induced in a dose-dependent manner by EtHg (Figure 3A). Splicing of Xbp1 mRNA began before 3 h and reached a maximum at 12 h after the initiation of treatment with 2 μM EtHg (Figure 3B). These results were confirmed by RT-qPCR (Figure 3C). The expression of Chop in cells treated with 2 μM EtHg reached a maximum (approximately 9.7 times greater than in control cells) at an early time point (within 3 h) and then decreased steadily until 24 h. However, the mRNA expression of Grp78 increased to a maximal level (approximately 5.1-fold greater than in control cells) at 12 h and then decreased 24 h after treatment with EtHg. mRNA expression of Erdj4, which is downstream of Xbp1, was elevated at 6 h and reached a maximal level (approximately 12.1-fold compared to the control) at 12 h. TM caused maximal increases in the mRNA expression levels of Chop (approximately 38.7-fold) and Grp78 (approximately 30.5-fold) at 12 h (Supplementary Figure 1B). Activation of the UPR leads to increases in the protein levels of GRP78, spliced XBP1, phospho-eIF2α, and CHOP. 12 h after EtHg treatment, GRP 78 protein levels

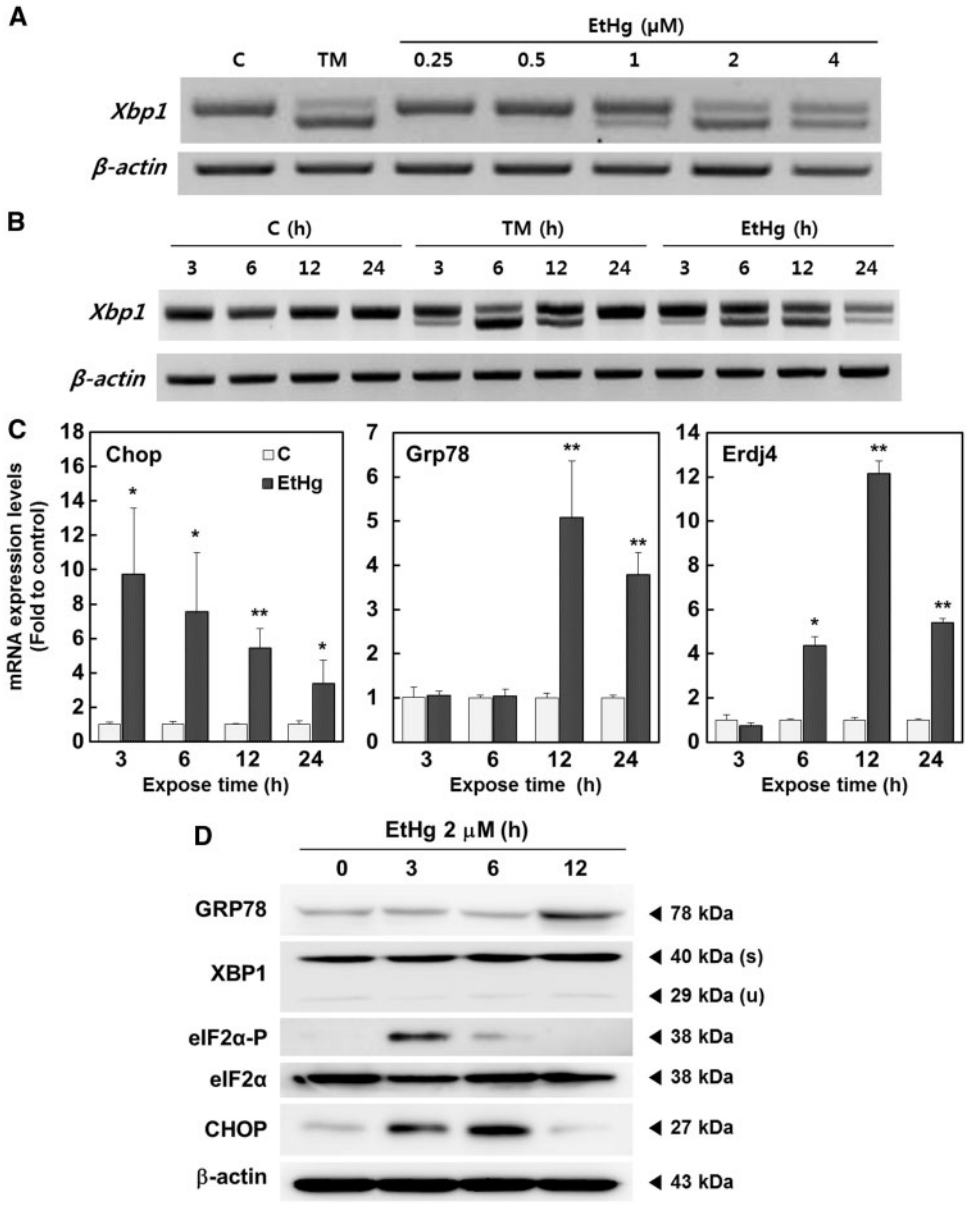


FIG. 3. Induction of ER stress by EtHg in HK-2 cells. A, Dose- and B, time-dependent alternative splicing of *Xbp1* mRNA in EtHg-treated HK-2 cells. For the dose-dependence experiment, the cells were treated with TM (10 ng/ml, positive control) or EtHg (0.25, 0.5, 1, 2, or 4 μM) for 6 h. For the time-dependence experiment, the cells were exposed to TM (10 ng/ml) or EtHg (2 μM) for 3, 6, 12, and 24 h. Alternatively spliced forms of *Xbp1* were analyzed using RT-PCR as described in the Materials and Methods section. C, Time-dependent changes in ER stress-related gene expression induced by 2 μM EtHg. Cells were treated with dimethylsulfoxide (DMSO, control) (white bar) or 2 μM EtHg (dark bar) for 3, 6, 12, and 24 h, and gene expression levels were determined in triplicate using an RT-qPCR assay. The data are presented as the means of 2 independent experiments. * indicates $p < 0.05$ and ** indicates $p < 0.01$ compared with untreated controls. D, Time-dependent changes in ER stress-related protein levels induced by EtHg. HK-2 cells were treated with 2 μM EtHg for 0, 3, 6, and 12 h and analyzed by immunoblotting using the indicated antibodies.

were elevated, whereas the level of phosphorylated eIF2α was significantly increased at 3 h and then gradually decreased until the 12 h time point. CHOP protein levels increased for the first 6 h after the addition of EtHg but began to decline at 12 h (Figure 3D). Collectively, the results show that EtHg induces ER stress not only *in vivo* in mouse kidney tissue, but also *in vitro* in human kidney HK-2 cells. In addition, the UPR is induced by EtHg in a dose- and time-dependent manner.

### *EtHg Induces ROS Production and Mitochondrial Dysfunction in HK-2 Cells*

Oxidative stress is the one of the major mechanisms of mercury-induced cellular toxicity and is closely related to ER stress. To measure ROS production, HK-2 cells were treated with various concentrations of EtHg (from 0.1 to 2 μM) for 3 h, and the production of ROS was quantified by FACS analysis. ROS production induced by 500 μM $H_2O_2$ (positive control) increased by approximately 40.9% compared with the control. EtHg treatment at 0.1, 0.5, 1, and 2 μM dose-dependently increased ROS production in the cells by 27.2%, 42.8%, 67.4% and 67.9%, respectively, compared with the control (Figure 4A). Even at the very low concentration of 0.1 μM, EtHg also induced the expression of metallothionein I (*MT-I*) and hydrogen peroxide-inducible clone (*Hic-5*) (Figure 4B), which are associated with the induction of oxidative stress. To assess the effect of EtHg on mitochondrial dysfunction, the mitochondrial membrane

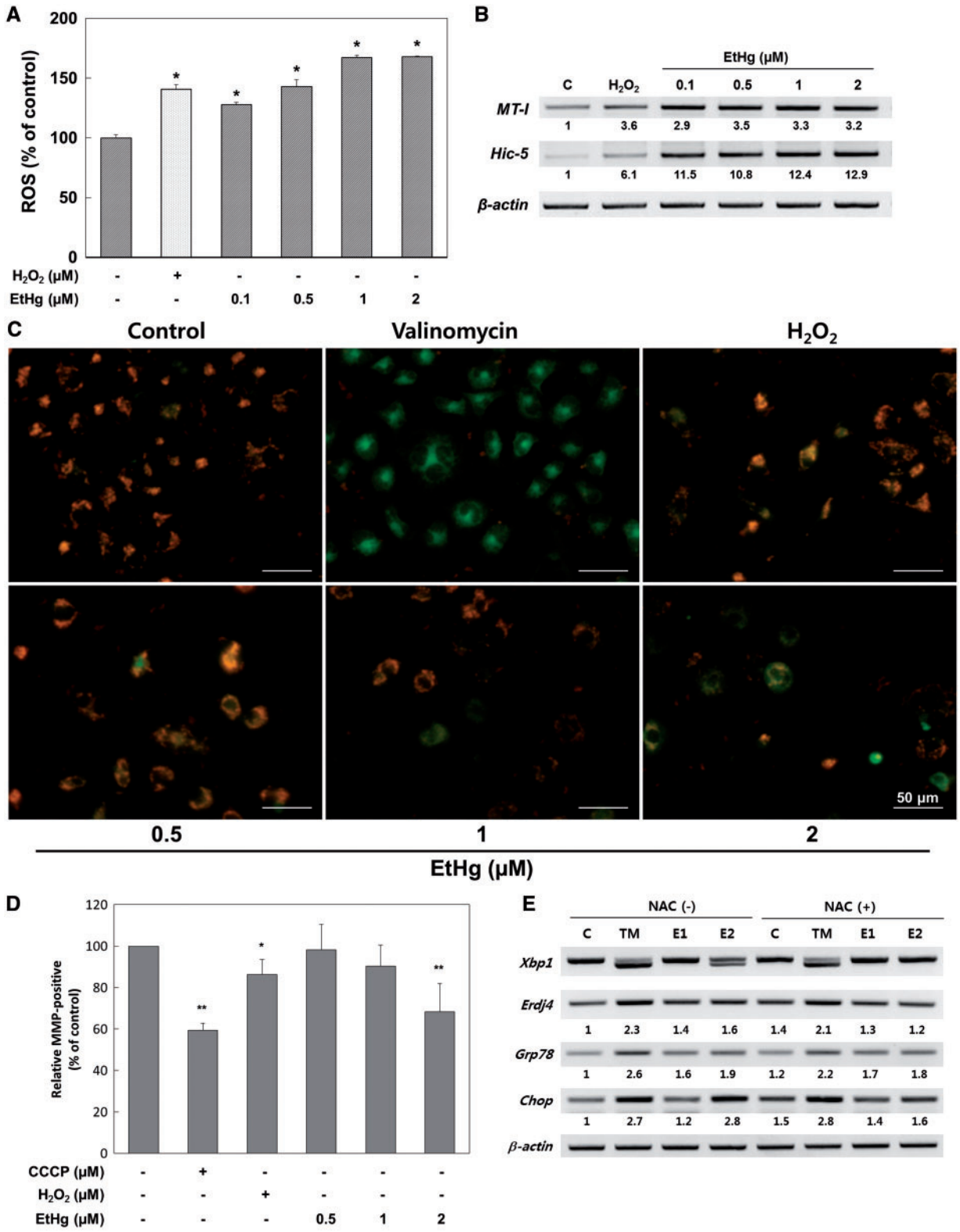


FIG. 4. Ethylmercury triggers oxidative stress and mitochondrial dysfunction in HK-2 cells. A, Dose-dependent changes in the production of intracellular ROS in HK-2 cells exposed to various concentrations of EtHg or $H_2O_2$. HK-2 cells were treated with 0.1 to 2 μM EtHg or 500 μM $H_2O_2$ for 3 h and then stained with the fluorescent dye carboxy-$H_2$DCFDA. ROS production was measured using flow cytometry as described in the Materials and Methods section. B, Effect of EtHg on the expression of ROS-related genes in HK-2 cells. Cells were treated with 500 μM $H_2O_2$ or 0.1, 0.5, 1, or 2 μM EtHg for 6 h and total RNA was prepared. The expression of the *MT-I* and *Hic*-5 genes was analyzed by semi-quantitative reverse transcription-polymerase chain reaction (RT-PCR). C, Representative fluorescent microscopic images of HK-2 cells stained with the fluorescence probe JC-1 after treatment with EtHg, valinomycin, or $H_2O_2$. Cells were treated with 500 μM $H_2O_2$, 1 μg/ml valinomycin, or various concentrations of EtHg for 24 h, stained with JC-1 for 20 min, and visualized under a fluorescent microscope. The experiments were repeated 3 times with similar results. D, Representative flow cytometry-based MMP profiles for EtHg-treated HK-2 cells. Cells were treated with 500 μM $H_2O_2$ or 0.5, 1, or 2 μM EtHg for 24 h. Data are presented as means ± SD (n = 4). E, The effects of EtHg on HK-2 cells the absence or presence of NAC (5 mM) for 24 h. RT-PCR analysis of ER stress-related gene expression levels.

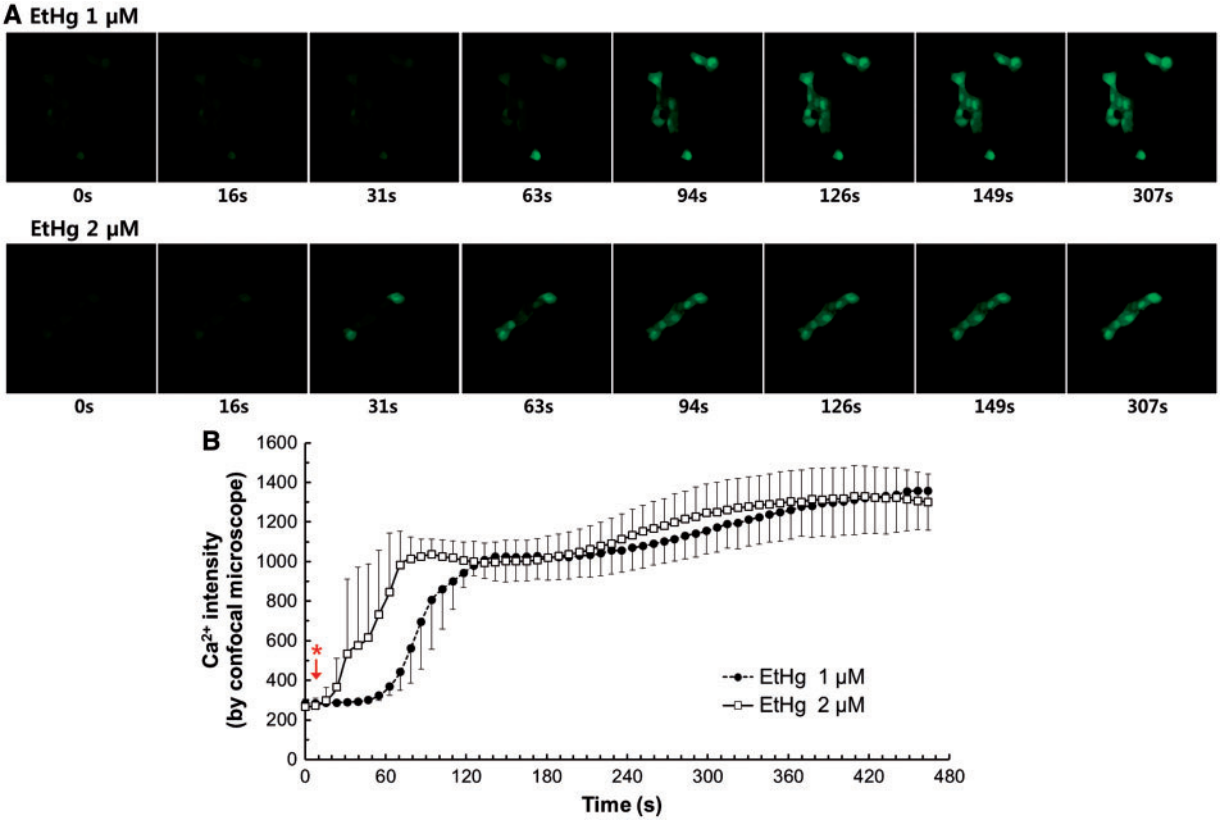


FIG. 5. EtHg stimulates $Ca^{2+}$ movement to the cytosol in HK-2 cells. The effects of EtHg on intracellular $Ca^{2+}$ mobilization in HK-2 cells were determined using confocal microscopy (A) and fluorescence quantitation of the confocal images (B) using ZEN software (Carl Zeiss, Germany). HK-2 cells were loaded with Fluo-3 AM for 30 min, EtHg (1 or 2 μM) was added (arrow), and cells were then imaged using confocal microscopy.

potential ($\Delta\psi_m$; MMP) was measured in HK-2 cells treated with 0.5, 1, and 2 μM EtHg. Exposure of the cells to EtHg increased the intensity of the green fluorescence associated with JC-1 monomer formation at low MMP compared with the control (Figure 4C). Figure 4D shows the percentages of $DiOC_2(3)$-positive staining following treatment with 500 μM $H_2O_2$ or EtHg (from 0.5 to 2 μM) for 24 h. The percentages of $DiOC_2(3)$-positive cells following treatment with 0.5, 1, and 2 μM EtHg were 98.1 ± 12.3, 90.4 ± 10.2 and 68.2 ± 13.6% ($n = 4$), respectively. The percentage of $DiOC_2(3)$-positive cells in the positive control (CCCP) and $H_2O_2$ groups were 59.3 ± 3.55 and 86.28 ± 7.33% ($n = 4$), respectively, after 24 h incubation. Taken together, these results demonstrate that EtHg treatment altered the MMP of HK-2 cells in a dose-dependent manner and 2 μM EtHg significantly decreased MMP.

To determine whether EtHg-induced oxidative stress triggers ER stress, HK-2 cells were simultaneously treated with N-acetyl cysteine (NAC, an antioxidant) and EtHg, and the degree of ER stress was compared with that of cells treated with EtHg alone (Figure 4E). Xbp1 splicing was observed in the cells treated with 2 μM EtHg but not in those co-treated with 2 μM EtHg and NAC. The expression of other ER stress-related genes was also reduced by co-treatment with NAC. The primary finding of this portion of the study is that EtHg-induced ER stress is partly mediated by oxidative stress in human renal proximal tubular HK-2 cells.

### *EtHg Stimulates $Ca^{2+}$ Release into the Cytosol in HK-2 Cells*

Cytosolic $Ca^{2+}$ signals have been implicated in the regulation of cell fate (Zheng *et al.*, 2013). ER stressors cause the release of $Ca^{2+}$ from ER stores, thus increasing the $Ca^{2+}$ concentration in the cytosol (Ullman *et al.*, 2008). Cells were loaded with a cytosolic $Ca^{2+}$-sensing dye and then placed into $Ca^{2+}$-free medium to assess intracellular $Ca^{2+}$ flux upon treatment with 1 or 2 μM EtHg. Cytosolic $Ca^{2+}$ signals started to increase at approximately 60 s and 30 s after the addition of 1 or 2 μM EtHg, respectively, and increased to a maximum of about 5.5-fold at both concentrations (Figs. 5A and B).

### *EtHg-Induced ER Stress and Oxidative Stress-Mediated Autophagy*

Several studies have reported that ER stress and oxidative stress are potent inducers of autophagy (Kawakami *et al.*, 2009). Therefore, the autophagic responses induced by EtHg were assessed in HK-2 cells. Cells treated with the autophagy inducer rapamycin, an mTOR inhibitor (Jung *et al.*, 2010), were used as a positive control. As shown in Figs 6A and B, the protein levels of Cathepsin B, Beclin 1, p62, and LC3B-II dose- and time-dependently increased in response to EtHg exposure. EtHg treatment also increased the number of LC3 puncta in NRK-52E/GFP_LC3 cells in a dose-dependent manner (Figure 6C).

To determine whether the autophagy induced by EtHg is mediated by ER stress, the effect of 4-phenylbutyric acid (4-PBA), a chemical chaperone that acts as a selective inhibitor of ER stress, on EtHg-induced autophagy was examined by monitoring the levels of Beclin 1 and LC3B-II. Treatment with EtHg alone strongly induced the expression of Beclin 1 and LC3B-II proteins, whereas co-treatment with EtHg and 4-PBA reduced the expression of both proteins in a time-dependent manner (Figs. 6D and E). Treatment with 4-PBA also blocked the formation of GFP-LC3 puncta induced by EtHg (Figure 6F). Next, to investigate the relationship between EtHg-induced ROS

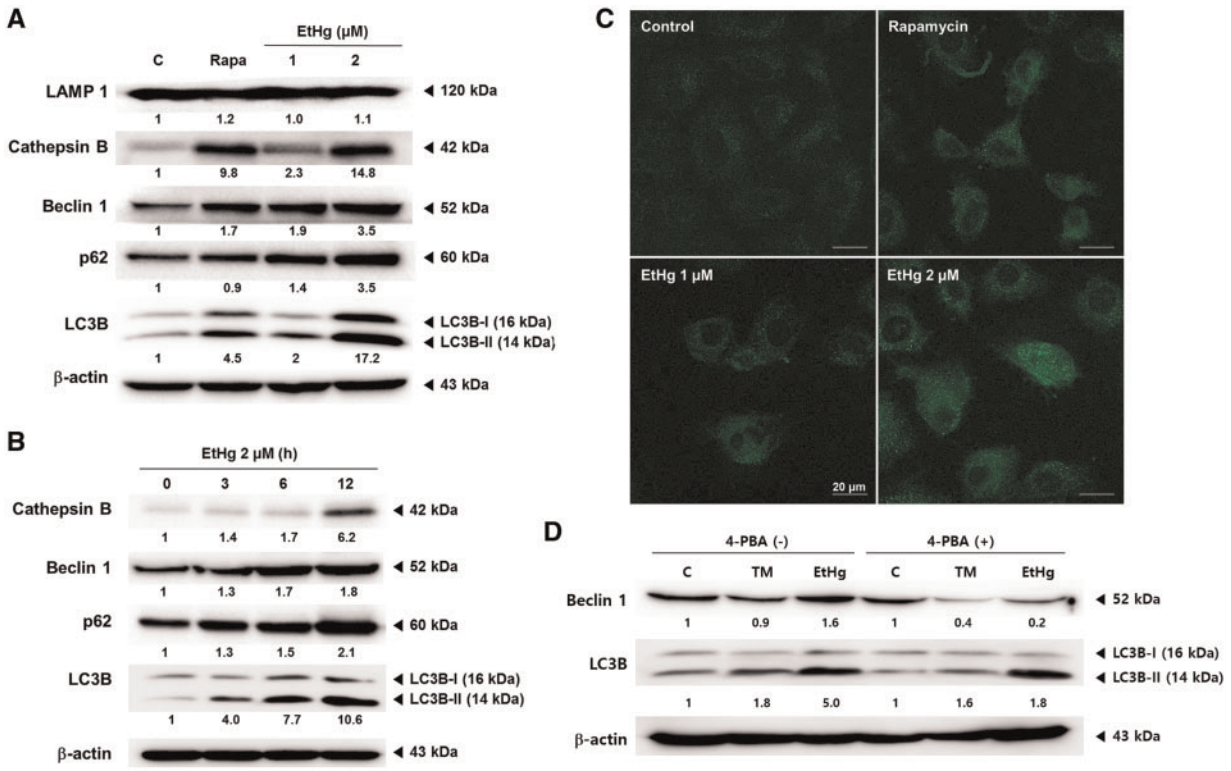


FIG. 6. EtHg induces autophagy in HK-2 cells. A, Dose- and B, time-dependent induction of autophagy by EtHg. In the dose-dependence experiment, the cells were treated with rapamycin (100 nM, positive control) or EtHg (1 or 2 μM) for 24 h. In the time-dependence experiment, cells were exposed to rapamycin (100 nM) or EtHg (2 μM) for 3, 6, and 12 h. Autophagy induction was determined by immunoblot analysis of Cathepsin B, Beclin 1, and p62 and LC3B conversion. C, Formation of LC3 puncta by EtHg. NRK-52E/GFP_LC3 cells were treated with 1 or 2 μM EtHg for 24 h and then fixed and observed using a confocal microscope. D, E, Inhibition of EtHg-induced autophagy by 4-PBA was determined by evaluating the levels of the autophagy marker protein and F, LC3 puncta formation. HK-2 cells were treated 2 μM EtHg with or without 2 mM 4-PBA for the indicated times, and autophagy was analyzed via immunoblotting. To measure LC3 puncta formation, NRK-52E/GFP_LC3 cells were treated with 1 or 2 μM EtHg or rapamycin (100 nM) with or without co-treatment with 2 mM 4-PBA for 24 h. Inhibition of EtHg-induced autophagy by G, trolox and H, I, NAC was analyzed by examining LC3-II levels and LC3 puncta formation as indicators of autophagy. HK-2 cells were treated with 2 μM EtHg with or without co-treatment with 100 μM trolox or 5 mM NAC for 24 h. To measure LC3 puncta formation, NRK-52E/GFP_LC3 cells were treated with 2 μM EtHg or rapamycin (100 nM) with or without co-treatment with 5 mM NAC for 24 h.

production and autophagy, the formation of LC3-II in HK-2 cells was observed after treatment with EtHg alone or in combination with trolox or NAC. Co-treatment with EtHg and trolox or NAC decreased the ratio of LC3B-II to actin (Figs. 6G and H) and reduced the number of GFP-LC3 puncta (Figure 6I). Together, these results indicate that both the ER stress and ROS generation induced by EtHg promote autophagic signaling in HK-2 cells.

### *Inhibition of Autophagolysosome Formation by EtHg*

To determine whether EtHg induces autophagosome accumulation through increased formation or decreased degradation of autophagosomes, autophagy flux in EtHg-treated cells was examined using different assays (Klionsky *et al.*, 2012). First, we treated NRK-52E/GFP-LC3 cells with rapamycin (positive control) or EtHg for 24 h to visualize the co-localization of autophagosomes and lysosomes via expression of GFP-LC3 puncta and lysosomes stained with Lysotracker. About 60.2% of GFP-LC3 puncta in rapamycin-treated cells co-localized with lysosomes, compared with about 7.04% in control cells (Figure 7A). The ratio of co-localization with lysosomes in 1 and 2 μM EtHg-treated cells was significantly lower, about 29.7 and 35.4%, respectively. Although 2 μM EtHg-treated cells contained more GLP-LC3 puncta than did rapamycin-treated cells, the co-localization ratio was significantly lower. Next, to examine whether the low ratio of autopahagosome and lysosome co-localization resulted from an imbalance between formation and degradation of autophagosomes, we examined cells treated with hydroxychloroquine (CQ), which blocks autophagosome degradation by altering lysosomal pH homeostasis, and wortmannin, which inhibits the formation of autophagosomes by inhibiting vacuolar protein sorting 34 (Vps34, which plays an important role in the vesicle nucleation process). To determine the number of newly formed autophagosomes, we incubated HK-2 cells with rapamycin or EtHg with or without CQ for 24 h and measured LC3-II by immunoblotting (Figure 7B). Control cells (both untreated and rapamycin-treated cells) and 1 μM EtHg-treated cells showed significant increases in LC3-II levels following CQ addition. In contrast, cells treated with 2 μM EtHg exhibited a slight increase in LC3-II levels with CQ co-treatment. Finally, to observe the inhibition of autophagosome degradation by EtHg, we treated NRK-52E/GFP-LC3 cells with rapamycin or 1 or 2 μM EtHg as follows: 1) only rapamycin or 1 or 2 μM EtHg for 24 h (w/o Wort), 2) rapamycin or 1 or 2 μM EtHg treatment for 24 h followed by addition of wortmannin for 1 h (→ Wort), and 3) rapamycin or 1 or 2 μM EtHg treatment with wortmannin for 24 h (w/ Wort) (Figure 7C). The number of GFP-LC3 puncta formed by rapamycin treatment was reduced by the addition of wortmannin, suggesting that autophagosomes formed by rapamycin treatment were continually subject to lysosomal degradation.

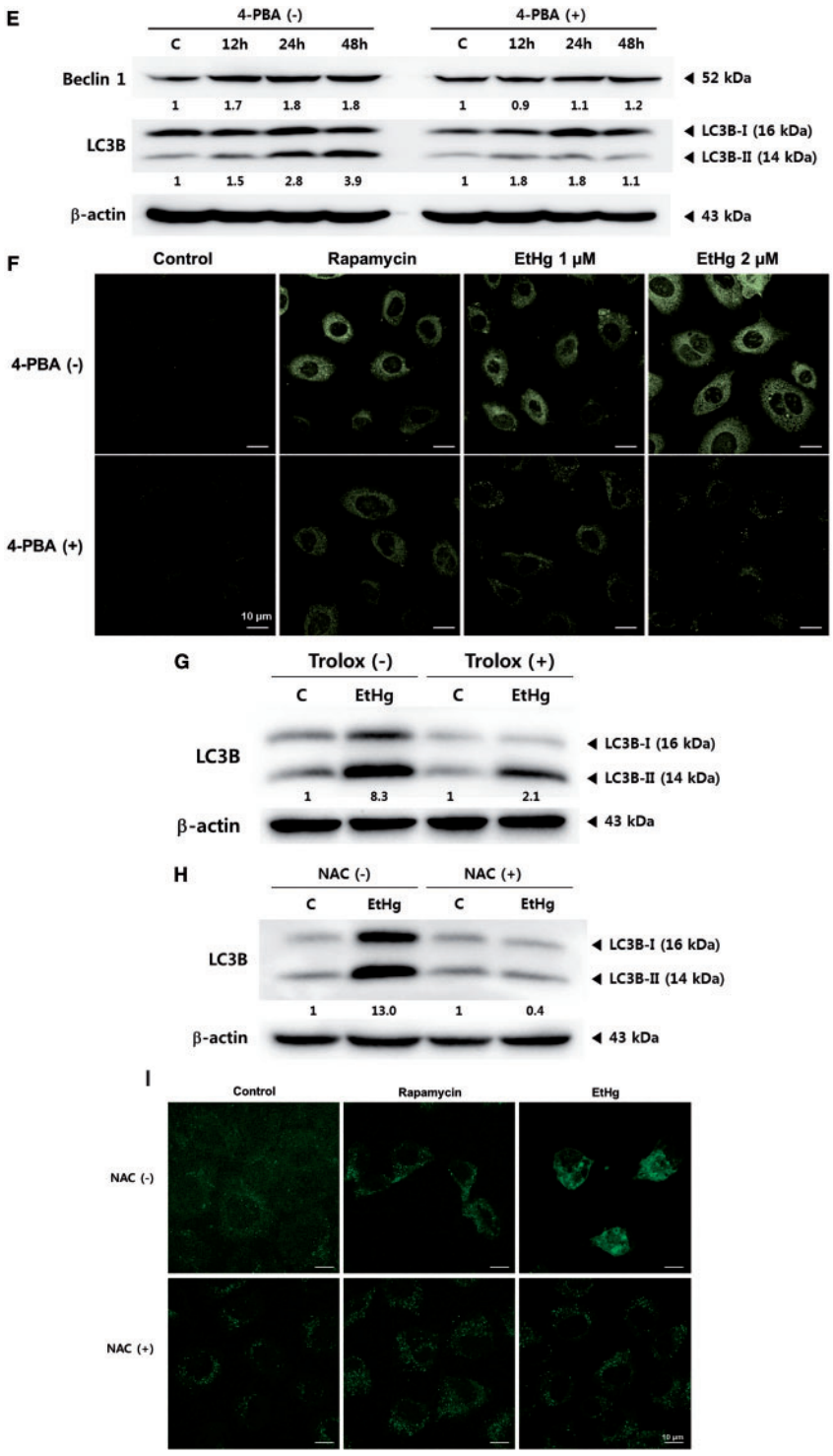


FIG. 6. Continued

In contrast, the number of EtHg-induced GFP-LC3 puncta was not reduced by wortmannin, which suggests that EtHg blocks the degradation of autophagosomes. These results collectively indicate that EtHg inhibits autophagic flux mainly by blocking fusion of autophagosomes and lysosomes.

We next aimed to determine how EtHg causes a defect in autophagic flux. Recently, autophagic SNARE syntaxin 17 (STX17) was shown to interact with SNAP29 and the lysosomal SNARE VAMP8, and all of these proteins are required for autophagosome–lysosome fusion in mammalian cells (Itakura *et al.*, 2012; Moreau *et al.*, 2013). Therefore, we focused on alterations in the protein levels of autophagosomal SNAREs (STX17, SNAP29 and VAMP8) by EtHg. Unexpectedly, these proteins were induced by treatment with rapamycin and a low dose of EtHg (1 μM) without any significant changes in gene expression (Supplementary Figure 2). However, the levels of these SNARE proteins in HK-2 cells treated with 2 μM EtHg were similar to those in untreated control cells (Figure 7D), even though

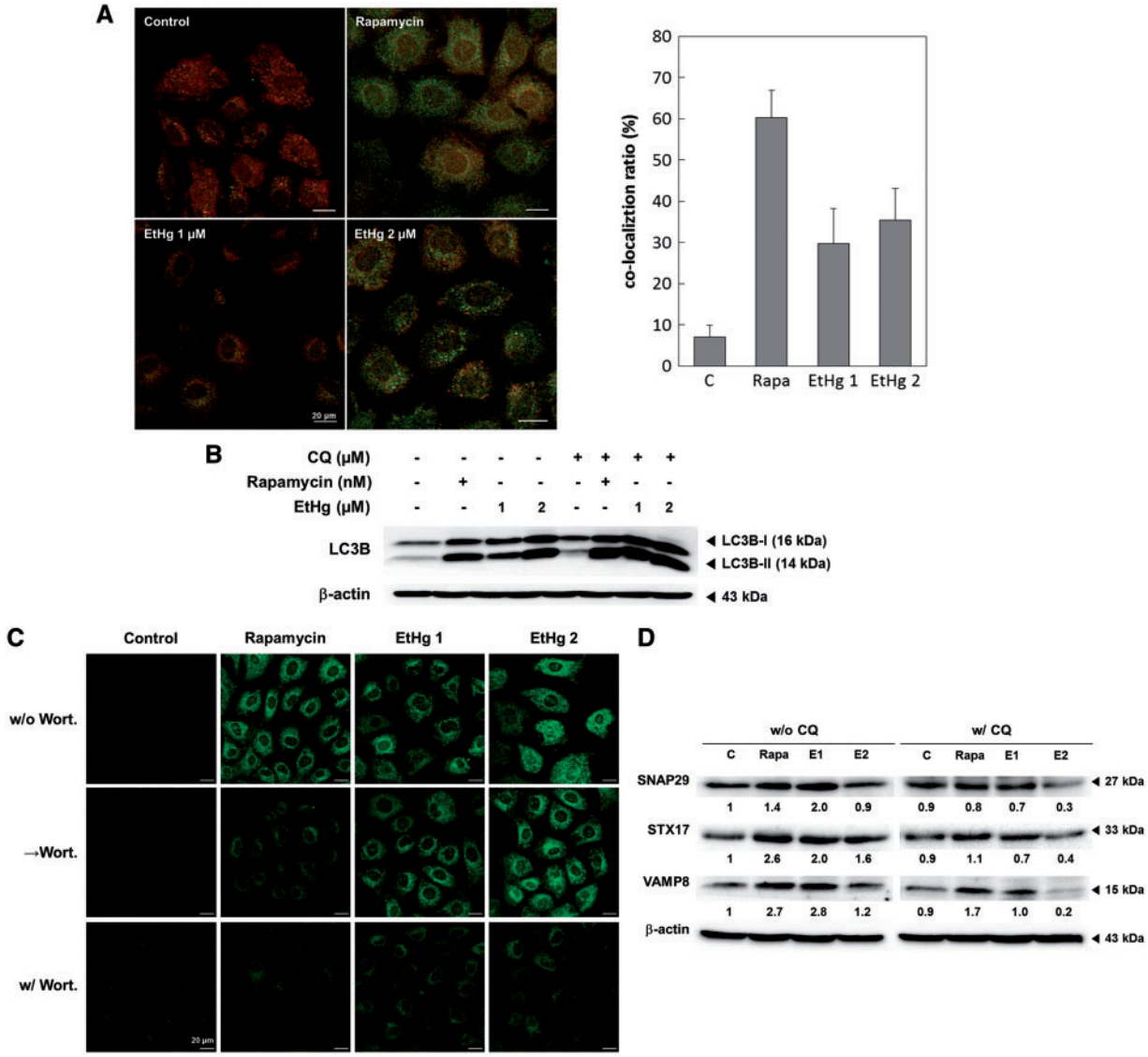


**FIG. 7.** EtHg blocks fusion of autophagosomes to lysosomes in HK-2 cells. A, NRK-52E/GFP_LC3 cells were treated with rapamycin (100 nM) or 1 or 2 μM EtHg for 24 h. Formation of acidic vesicular organelles was monitored by LysoTracker DND-99. Note the yellow color, showing the co-localization of GFP-LC3 puncta (green) and LysoTracker DND-99 (red). Quantitation of data represented in (A) showing the mean percentage ± SD, from 4 independent experiments, of LC3 structures co-localizing with lysosome ($n = 10$). Scale bar, 20 μm. B, HK-2 cells were treated with rapamycin (100 nM) or 1 or 2 μM EtHg for 24 with or without 5 μM CQ (Chloroquine, 2h pre-incubation), and analyzed using immunoblotting. C, NRK-52E/GFP_LC3 cells were treated with rapamycin (100 nM) or 1 or 2 μM EtHg (w/o Wort.), rapamycin (100 nM) or 1 or 2 μM EtHg for 24 h followed by addition of 50 nM wortmannin for 1 h (→ Wort.) or rapamycin (100 nM) or 1 or 2 μM EtHg with 50 nM wortmannin together for 24 h (w/ Wort.). Scale bar, 20 μm. D, HK-2 cells were treated with rapamycin (100 nM) or 1 or 2 μM EtHg for 24 h, and the levels of SNARE proteins (STX17, SNAP29 and VAMP8) were analyzed using immunoblotting.

autophagosome formation was significantly increased by EtHg treatment (Figs. 6 A and C).

Next, we asked whether the levels of these SNARE proteins were related to reduced cell viability via inhibition of autophagosome flux. Co-treatment with rapamycin or EtHg (1 and 2 μM) and CQ decreased cell viability and the levels of SNARE proteins compared with treatment with each chemical alone (Figs. 7D and 8A). Although more detailed experiments are required to elucidate these findings, this experiment demonstrated that EtHg affects the protein levels of STX17, SNAP29, and VAMP8 by at least in part by inhibiting autophagosome–lysosome fusion.

### *Induction of Necrosis by EtHg*

In order to explore how inhibition of autophagic flux brings about cell death, the type of cell death was examined in HK-2 cells co-treated with EtHg or rapamycin and CQ (Figure 8A). Co-treatment of rapamycin or EtHg (1 or 2 μM) with CQ increased cell death by 30.2, 21.3, and 25.2%, respectively, compared with treatment with each chemical alone. 1 or 2 μM EtHg-treated HK-2 cells exhibited cell death in a dose-dependent manner. Following treatment with 1 μM EtHg, the number of surviving cells was reduced by approximately 20.5% and the number of apoptotic cells was increased by approximately 1.6% compared with the untreated control. However, the necrotic cell population was dramatically increased to 32.3% of all cells following treatment with 2 μM EtHg. In untreated control cells, CQ treatment slightly increased the necrotic cell population; however, the number of apoptotic cells did not change. Following rapamycin treatment, CQ-induced apoptotic and necrotic cell death were increased by approximately 1.3% and 10.9%, respectively. In cells treated with 1 and 2 μM EtHg,

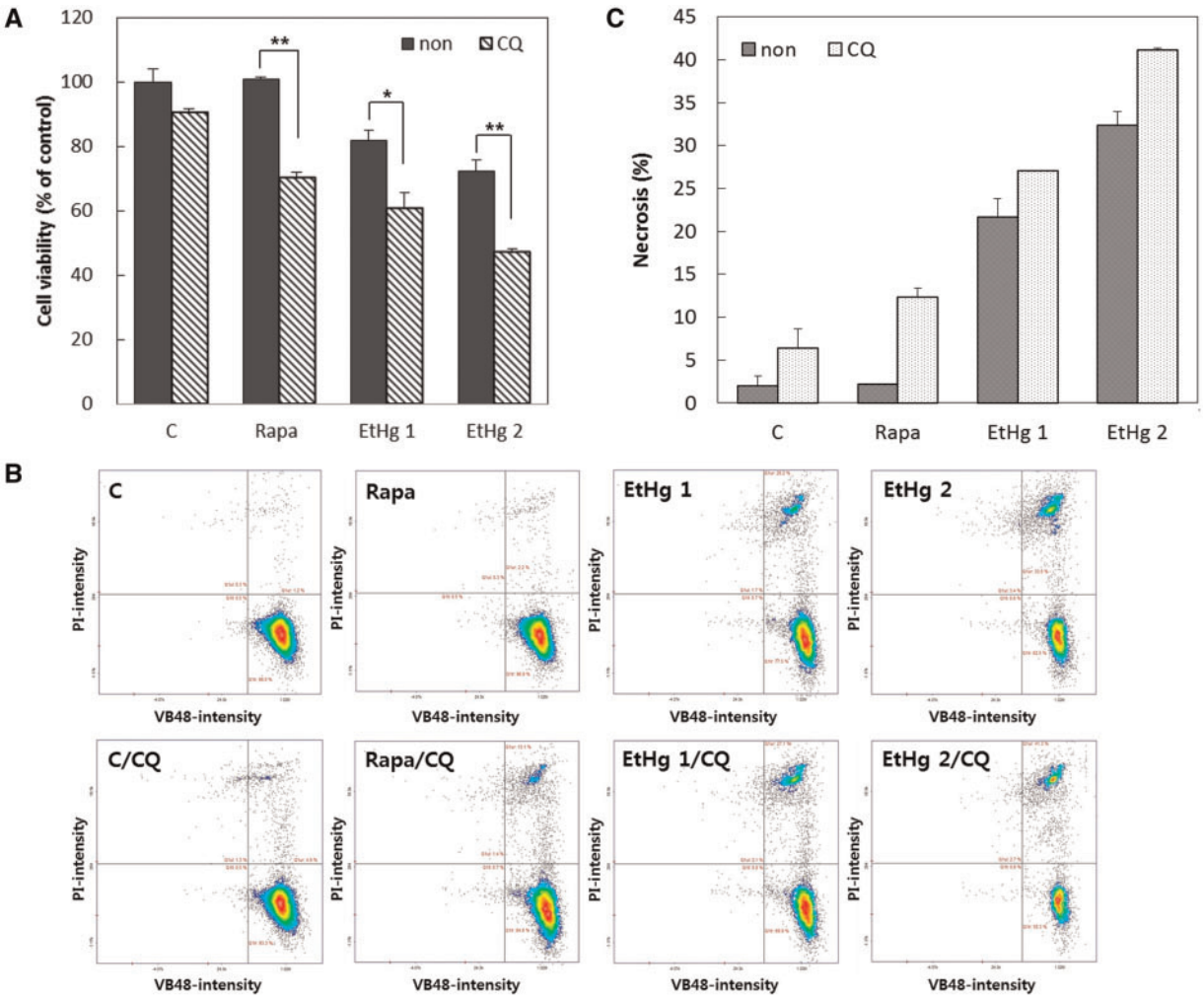


FIG. 8. High doses of EtHg induce necrosis in HK-2 cells. A, HK-2 cells were treated with rapamycin (100 nM) or 1 or 2 μM EtHg for 24 h with or without 5 μM CQ (2 h pre-incubation), and cell viability was measured using the MTS assay. *$P < 0.05$ and **$P < 0.01$ compared with untreated controls. B, Effect of EtHg on cell vitality. HK-2 cells were treated with 1 or 2 μM EtHg for 24 h with or without 5 μM CQ (2 h pre-incubation), and cell vitality was determined using a NucleoCounter NC-250™ instrument. C, Quantitation of the vitality data in (B) showing EtHg-induced necrosis by CQ. D, Immunoblot analysis of HMGB1 in the supernatants (upper panel, media) and cell lysates (lower panel) of the HK-2 cells treated with rapamycin (100 nM) or EtHg (1 or 2 μM) for 24 h. E, Inhibition of cell death in Hk-2 cells treated with 1 or 2 μM EtHg or rapamycin (100 nM) for 24 h by various doses of necrostatin-1. Cell viability was determined using the MTS assay. F, A schematic diagram of a potential mechanistic pathway for the toxic dose EtHg-induced kidney damage.

the percentage of necrotic cells increased to 6.9% and 7.8%, respectively, with the addition of CQ (Figs. 8B and C). To confirm these cell death results, alterations in necrosis- and apoptosis-related proteins by EtHg were observed by immunoblotting. Levels of the archetypal necrosis marker HMGB1 dose-dependently increased in response to EtHg treatment in HK-2 cells (Figure 8D). In contrast, EtHg weakly triggered apoptosis via caspase 9 and 12 in HK-2 cells (Supplementary Figure 3). These results indicate that inhibition of autophagosome–lysosome fusion increases necrotic cell death. To confirm EtHg-induced necrosis, we used necrostatin-1, an inhibitor of necroptosis, which blocks a critical step in necroptosis. Necrostatin-1 significantly inhibited the cell death induced by EtHg in a dose-dependent manner (Figure 8E). These data suggest that EtHg partially blocks fusion of autophagosomes with lysosomes, which stimulated necrosis in HK-2 cells.

## DISCUSSION

Mercury (Hg) is a highly toxic and redox-active heavy metal; Hg-related pathologies include renal injury and neuronal disorders. Although MeHg is regarded as the most toxic of all organic mercury derivatives in animals and humans (Brockman *et al.*, 2011; Sumathi *et al.*, 2012), in the present study, EtHg was shown to be the most cytotoxic of the 5 organic mercury compounds (MBH, DBM, DPM, MeHg, EtHg) tested in the human renal proximal tubule HK-2 cell line. This *in vitro* EtHg toxicity is consistent with a report that the cytotoxicity of sodium ethylmercurithiosalicylate was greater than that of MeHg as indicated by $EC_{50}$ values determined using an MTT assay in 2 kidney cell lines (MDCK and LLC-PK1) and primary cultures of human proximal tubular cells (Bohets *et al.*, 1995). Therefore, we studied the mechanism of EtHg-induced renal toxicity with a focus on autophagy.

Recently, studies of many toxic metals, including cadmium and arsenic, have demonstrated that ER stress can mediate cellular dysfunction and cell death during the progression of several diseases (Kitamura and Hiramatsu, 2010; Lu *et al.*, 2011). Autophagy has been shown to be the initial response of a cell to toxic metals in a concentration- and time-dependent manner (Chatterjee *et al.*, 2014b). Autophagy is induced in renal tubular cells during acute kidney injury; however, whether this is

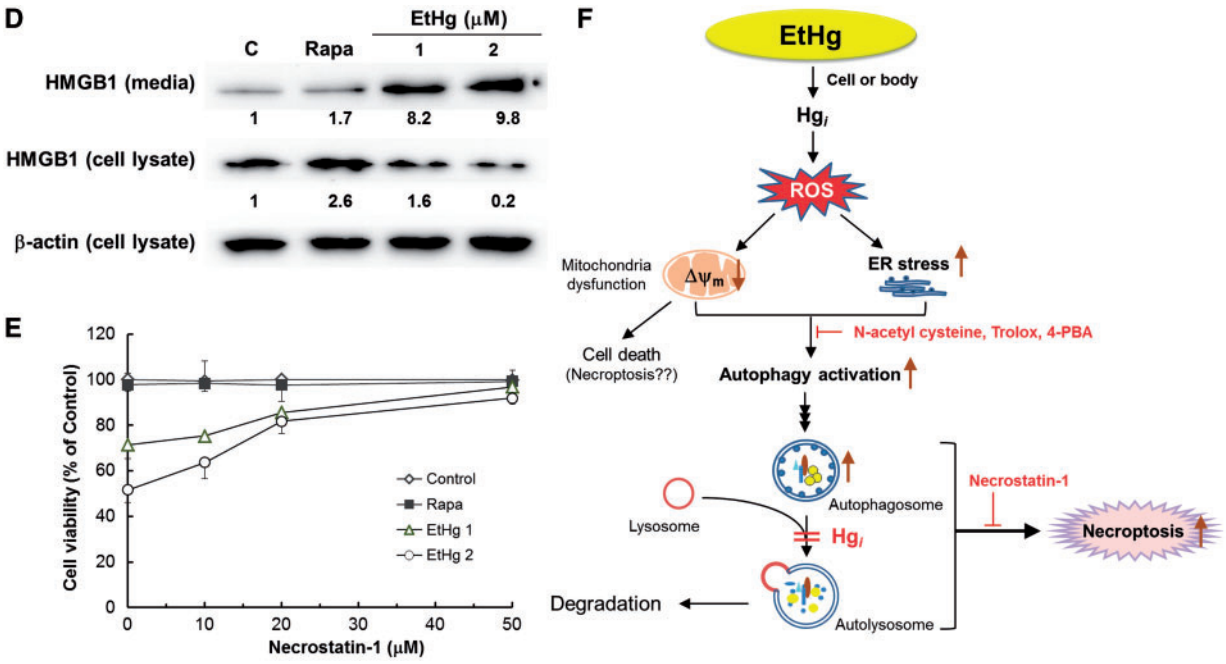


FIG. 8. Continued.

protective or injurious remains controversial (Jiang *et al.*, 2012). In this study, kidney tissues of mice exposed to various doses of EtHg (1, 2, 5, and 10 mg/kg for 5 days) exhibited autophagy with or without pathological changes depending on the dose of EtHg (Figure 2). These results are consistent with the hypothesis that autophagy plays a dual role in renal ischemia-reperfusion injury (IRI), having both protective and detrimental properties, depending on the duration of the ischemic period and the phase of the IRI process. Others have reported that optimal autophagy modulation restricts autophagy levels inside a protective therapeutic window that depends on the extent of IRI (Decuypere *et al.*, 2015). High-dose EtHg exposure may surpass the threshold at which autophagy is beneficial and becomes detrimental to kidney tissue. However, the kidney tissues of mice exposed to subtoxic levels of EtHg exhibited not only autophagy but also ER stress without any notable histopathological changes. Therefore, ER stress and autophagy seem to be initial, protective responses of kidney cells to exposure to subtoxic doses of EtHg. Chargui *et al.* (2011) proposed that the autophagy pathway could serve as a new, sensitive biomarker of renal injury after exposure to subtoxic doses of Cd. Similarly, autophagosome formation and the UPR response after exposure to subtoxic doses of EtHg seem to be sensitive markers of kidney damage.

Although the role of autophagy in metal-induced toxicity has not been extensively studied, metals and metal nanoparticles were reported to induce autophagy. However, different metals have unique features and physicochemical properties that confer specific toxicological mechanisms of action (Chatterjee *et al.*, 2014b). In our *in vitro* studies in HK-2 cells, EtHg exposure induced autophagy as assessed by LC3 II protein levels, autophagic protein levels, and cellular LC3 puncta; it also induced ER stress not only at a low concentration (1 μM), which produced limited cytotoxicity, but also at a high concentration (2 μM), which resulted in about 45% cytotoxicity after a 24-h incubation (Figure 1). These *in vitro* results were similar to those observed in the kidney tissues of mice treated with EtHg. Low doses of EtHg induced autophagy in HK-2 cells and mouse kidney tissue. Autophagy is also thought to be the initial response of cells to other heavy metals such as arsenic and cadmium (Bolt *et al.*, 2010; Kanzawa *et al.*, 2003) and mercury in rat hepatocytes (Chatterjee *et al.*, 2014a).

Several studies have demonstrated that reactive oxygen species (ROS) production and oxidative stress play a key role in the toxicity and carcinogenicity of metals (Tchounwou *et al.*, 2012). Despite the absence of incontrovertible evidence, it is reasonable to propose that mercury induces endoplasmic reticulum stress (Tinkov *et al.*, 2015). EtHg-treated cells exhibited time-dependent expression of UPR-related proteins such as phosphorylated eIF2α, CHOP, GRP78, and spliced XBP1 (Figure 3D), and seemed to exhibit activation of all 3 arms of the UPR. In addition, EtHg exposure induced *MT-I* and *Hic-5* transcription and damaged the mitochondrial membrane potential in parallel with an increase in ROS levels in HK-2 cells (Figure 4). The accumulation of LC-3 II induced by EtHg was significantly reduced by 4-PBA (a chemical chaperone), trolox (an antioxidant), and NAC (an antioxidant precursor for the biosynthesis of GSH); NAC most effectively decreased the autophagic response compared with trolox and 4-PBA. These results suggest that EtHg-induced autophagy is mediated by oxidative and ER stress in HK-2 cells. Interestingly, EtHg-induced cytotoxicity was completely prevented by NAC treatment but not by treatment with either trolox or 4-PBA (Supplementary Figure 4). NAC significantly inhibited the UPR response induced by EtHg, but not by tunicamycin (Figure 4E). These results are in agreement with those of previous reports which showed that toxicity caused by mercury exposure appears to be mediated by mitochondrial damage via depletion of GSH, coupled with binding to thiol groups (-SH), which generates free radicals (Carocci *et al.*, 2014). Mercury has a high affinity for thiol groups that are present in amino acids such as cysteine and *N*-acetyl cysteine, lipoic acid, proteins, and enzymes. NAC can prevent the depletion of cellular GSH by EtHg, and thus protect the cell against damage from antioxidant enzymes. In addition, the depletion of cellular thiol

groups by EtHg seemed to be critical not only for cytotoxicity but also for ER stress- and oxidative stress-induced autophagy.

Autophagy, which has been proposed as a third mode of cell death, along with apoptosis and necrosis, is a process in which cells generate energy and metabolites by digesting their own damaged or harmful cytoplasmic components and organelles (Kroemer and Levine, 2008). Under various environmental or cellular stresses, autophagy is a tightly regulated adaptive mechanism that helps cells survival. Cargo incorporation occurs during autophagosome maturation. The adaptor protein p62 targets ubiquitinated proteins for transport to autophagosomes for their eventual degradation in autolysosomes and is used as a marker of autophagic flux (Bjorkoy *et al.*, 2005; Kirkin *et al.*, 2009). When autophagy is arrested, p62 levels increase. In this study, we measured the protein levels of LC3-II and p62 as specific markers for autophagy in HK-2 cells. We observed that LC3-II expression in EtHg-treated HK-2 cells was dose-dependently increased in proportion to p62 levels without alterations in the levels of LAMP1. This result suggests that EtHg can arrest autophagic flux. Co-localization of autophagosomal and lysosomal markers in EtHg-treated cells was remarkably decreased compared with that in rapamycin-treated cells (Figs. 6A and 7A). In contrast to rapamycin, wortmannin treatment of cells pretreated with EtHg did not decrease the number of LC3 puncta compared to the number in cells treated with EtHg alone (Fig. 7C). These results indicate that EtHg blocks autophagic flux in kidney cells. This is the first report that mercury inhibits autophagic flux. In addition, LC3-II formation was significantly increased by co-treatment of rapamycin or 1 μM EtHg with CQ, while not by co-treatment with 2 μM EtHg and CQ. This result suggests that EtHg can inhibit autophagic flux in a dose-dependent manner. Cell viability was markedly decreased following treatment with 2 μM EtHg compared with 1 μM EtHg (Figure 1). Activation of autophagy is a double-edged sword. On the one hand, autophagy is essential for provoking a protective response and enhancing a cell's adaptation to metabolic stressors and immunological challenges. On the other hand, excessive autophagic activation, derailed autophagic trafficking, or imbalanced degradation and recycling can give rise to pathogenic conditions by straining critical cellular constituents, leading to cell degeneration and toxicity (Liang, 2010). Therefore, high concentrations of EtHg in cells induced excessive autophagic activation, and autophagosome accumulation owing to strong inhibition of autophagic flux seems to have overwhelmed the protective nature of autophagy and contributed to kidney cell damage.

Although our knowledge of the mechanisms of membrane fusion during autophagosome formation is limited, it is known that a set of SNARE proteins, including STX17, SNAP29, and VAMP8, are essential for the fusion of autophagosomes and lysosomes (Liu *et al.*, 2015). Interestingly, EtHg and rapamycin treatment altered the protein levels of autophagosomal SNAREs (STX17, SNAP29, and VAMP8) without affecting their mRNA levels. Treatment of HK-2 cells with rapamycin or 1 μM EtHg induced the expression of those SNAREs, while cells treated with a high, cytotoxic concentration of EtHg (2 μM) did not exhibit alterations in their levels. It remains unclear whether these SNAREs are fusion competents and how their fusogenic activity is specifically regulated during autophagy (Liu *et al.*, 2015). Although this issue requires more detailed experiments, autophagy inducers such as EtHg and rapamycin seemed to increase the levels of SNARE proteins, stimulate autophagosome-lysosome fusion, and protect the cells from toxicity. Co-treatment of CQ with EtHg or rapamycin led to a decrease in cell viability and the cellular levels of SNARE proteins (Figs. 7D and 8A). These results suggest that the increased concentration of autophagosomes following inhibition of autophagic flux can exacerbate cellular damage and result in a blockade of the increase in SNARE protein levels by autophagy inducers in HK-2 cells.

Mercury treatment has been shown to induce apoptosis, necrosis, and autophagy in different cell types (Vergilio *et al.*, 2015), and organic and inorganic Hg species differ in their mechanisms of toxicity in the different cell types (Lohren *et al.*, 2015). The majority of studies have focused on the mechanisms of mercury-induced apoptosis. The ER plays an important role in regulating apoptosis by adjusting the load of $Ca^{2+}$ imposed upon the mitochondria (Scorrano *et al.*, 2003) and by inducing CHOP. Furthermore, ER stress-induced cell death/apoptosis can be induced by ASK1-JNK (c-Jun N-terminal kinase) signaling downstream from the IRE1 sensor (Geier *et al.*, 2007). EtHg-induced cell death in a time- and concentration-dependent manner. Exposure of HK-2 cells to a high dose of EtHg increased cellular $Ca^{2+}$ levels very quickly and induced a sustained increase in the levels of CHOP protein (Figure 3). However, the number of apoptotic cells was only slightly increased compared with untreated cells (Supplementary Figure 2), and JNK phosphorylation was unchanged (data not shown). In the absence of apoptotic signaling, mercury species are capable of activating nonapoptotic death pathways, such as necroptosis (Vanden Berghe *et al.*, 2014). Low concentrations or shorter times of exposure to EtHg induced autophagy without significant cytotoxicity, suggesting that this process serves to enhance cell survival. However, higher concentrations or longer times of exposure to EtHg induced more intensive autophagy, followed by inhibition of autophagosome-lysosome fusion, and seemed to result in cellular necrosis. In fact, HMGB1 release stimulated by EtHg treatment increased dose-dependently (Figure 8D). In the vitality assay, after treatment with EtHg, the number of necrotic cells was found to be increased dose-dependently. In addition, necrotic cell death was significantly increased by cotreatment of CQ not only with rapamycin but also with EtHg. In addition, necrostatin-1 blocked EtHg-induced cytotoxicity in HK-2 cells (Figure 8). Therefore, although EtHg treatment of HK-2 cells induced several apoptosis-related cellular phenomena, EtHg-induced cell death mainly by autophagy and necrosis, depending on dose.

In this study, we reported that low concentrations of EtHg-induced autophagy rather than apoptosis and that this process involves oxidative stress and ER stress without cell damage in *in vitro* and *in vivo* models. In addition, longer exposure times to low or high concentrations of EtHg caused cellular necrosis by blocking the fusion of autophagosomes to lysosomes and resulted in kidney cell damage (Figure 8F). We suggest that autophagy may play a dual role in EtHg-induced kidney cell toxicity, being both protective at low doses and exacerbating at high doses. Although we employed low and high doses of EtHg in the *in vivo* experiments, we exposed the mice to relatively high doses of EtHg (1–10 mg/kg) to induce renal damage. The dose was adapted to the mouse body weight (FDA CEDR, 2005), and corresponded to a dose 20.6–206 times higher than that the amount of Hg a 3.5-month-old human baby receives from vaccines (Clements, 2004). EtHg has been shown to have a shorter half-life in blood than MeHg in an *in vivo* animal model (Dorea *et al.*, 2013), the *in vitro* cytotoxicity of EtHg was the strongest among 5 organic mercuric compounds tested, including MeHg, in the HK-2 human kidney cell line. Therefore, simultaneous exposure to EtHg, even at subtoxic doses, and other mercurial compounds might result in enhanced toxic effects such as tubular cell necrosis.

## SUPPLEMENTARY DATA

Supplementary data are available online at http://toxsci.oxfordjournals.org/.

## Funding

This research was supported by a grant from the Ministry of Food and Drug Safety (10182KFDA992-1101), a Korean Healthcare Technology R&D Project grant funded by the Ministry for Health, Welfare & Family Affairs (A100096), Republic of Korea, and by a grant from Korea University.

## References

Amaya, C., Fader, C. M., and Colombo, M. I. (2015). Autophagy and proteins involved in vesicular trafficking. *FEBS Lett.* **589**, 3343–3353.

Bjorkoy, G., Lamark, T., Brech, A., Outzen, H., Perander, M., Overvatn, A., Stenmark, H., and Johansen, T. (2005). p62/SQSTM1 forms protein aggregates degraded by autophagy and has a protective effect on huntingtin-induced cell death. *J. Cell Biol.* **171**, 603–614.

Bohets, H. H., Van Thielen, M. N., Van der Biest, I., Van Landeghem, G. F., D'Haese, P. C., Nouwen, E. J., De Broe, M. E., and Dierickx, P. J. (1995). Cytotoxicity of mercury compounds in LLC-PK1, MDCK and human proximal tubular cells. *Kidney. Int.* **47**, 395–403.

Bolt, A. M., Douglas, R. M., and Klimecki, W. T. (2010). Arsenite exposure in human lymphoblastoid cell lines induces autophagy and coordinated induction of lysosomal genes. *Toxicol. Lett.* **199**, 153–159.

Brockman, J. D., Raymond, L. J., Ralston, C. R., Robertson, J. D., Bodkin, N., Sharp, N., and Ralston, N. V. (2011). The nail as a noninvasive indicator of methylmercury exposures and mercury/selenium molar ratios in brain, kidney, and livers of Long-Evans rats. *Biol. Trace Elem. Res.* **144**, 812–820.

Carocci, A., Rovito, N., Sinicropi, M. S., and Genchi, G. (2014). Mercury toxicity and neurodegenerative effects. *Rev. Environ. Contam. Toxicol.* **229**, 1–18.

Chang, S. H., Lee, H. J., Kang, B., Yu, K. N., Minai-Tehrani, A., Lee, S., Kim, S. U., and Cho, M. H. (2013). Methylmercury induces caspase-dependent apoptosis and autophagy in human neural stem cells. *J. Toxicol. Sci.* **38**, 823–831.

Chargui, A., Zekri, S., Jacquillet, G., Rubera, I., Ilie, M., Belaid, A., Duranton, C., Tauc, M., Hofman, P., Poujeol, P., El May, M.V., Mograbi, B. (2011). Cadmium-induced autophagy in rat kidney: an early biomarker of subtoxic exposure. *Toxicol. Sci.* **121**, 31–42.

Chatterjee, S., Ray, A., Mukherjee, S., Agarwal, S., Kundu, R., and Bhattacharya, S. (2014a). Low concentration of mercury induces autophagic cell death in rat hepatocytes. *Toxicol. Ind. Health* **30**, 611–620.

Chatterjee, S., Sarkar, S., and Bhattacharya, S. (2014b). Toxic metals and autophagy. *Chem. Res. Toxicol.* **27**, 1887–1900.

Clarkson, T. W., and Magos, L. (2006). The toxicology of mercury and its chemical compounds. *Crit. Rev. Toxicol.* **36**, 609–662.

Clements, C. J. (2004). The evidence for the safety of thiomersal in newborn and infant vaccines. *Vaccine* **22**, 1854–1861.

Decuypere, J. P., Ceulemans, L. J., Agostinis, P., Monbaliu, D., Naesens, M., Pirenne, J., and Jochmans, I. (2015). Autophagy and the Kidney: Implications for Ischemia-Reperfusion Injury and Therapy. *Am. J. Kidney. Dis.* **66**, 699–709.

Dorea, J. G., Farina, M., and Rocha, J. B. (2013). Toxicity of ethylmercury (and Thimerosal): a comparison with methylmercury. *J. Appl. Toxicol.* **33**, 700–711.

FDA CDER (2005) Guidance for Industry; Estimating the Maximum Safe Starting Dose in Initial Clinical Trials for Therapeutics in Adult Healthy Volunteers, pp27

Geier, D. A., Sykes, L. K., and Geier, M. R. (2007). A review of Thimerosal (Merthiolate) and its ethylmercury breakdown product: specific historical considerations regarding safety and effectiveness. *J. Toxicol. Environ. Health. B Crit. Rev.* **10**, 575–596.

Grotto, D., Valentini, J., Fillion, M., Passos, C. J., Garcia, S. C., Mergler, D., and Barbosa, F. Jr. (2010). Mercury exposure and oxidative stress in communities of the Brazilian Amazon. *Sci. Total Environ.* **408**, 806–811.

Itakura, E., Kishi-Itakura, C., and Mizushima, N. (2012). The hairpin-type tail-anchored SNARE syntaxin 17 targets to autophagosomes for fusion with endosomes/lysosomes. *Cell* **151**, 1256–1269.

Jiang, M., Wei, Q., Dong, G., Komatsu, M., Su, Y., and Dong, Z. (2012). Autophagy in proximal tubules protects against acute kidney injury. *Kidney. Int.* **82**, 1271–1283.

Jung, C. H., Ro, S. H., Cao, J., Otto, N. M., and Kim, D. H. (2010). mTOR regulation of autophagy. *FEBS Lett.* **584**, 1287–1295.

Kanzawa, T., Kondo, Y., Ito, H., Kondo, S., and Germano, I. (2003). Induction of autophagic cell death in malignant glioma cells by arsenic trioxide. *Cancer. Res.* **63**, 2103–2108.

Kawakami, T., Inagi, R., Takano, H., Sato, S., Ingelfinger, J. R., Fujita, T., and Nangaku, M. (2009). Endoplasmic reticulum stress induces autophagy in renal proximal tubular cells. *Nephrol. Dial. Transplant* **24**, 2665–2672.

Kirkin, V., McEwan, D. G., Novak, I., and Dikic, I. (2009). A role for ubiquitin in selective autophagy. *Mol. Cell* **34**, 259–269.

Kitamura, M., and Hiramatsu, N. (2010). The oxidative stress: endoplasmic reticulum stress axis in cadmium toxicity. *Biometals* **23**, 941–950.

Klionsky, D. J., Abdalla, F. C., Abeliovich, H., Abraham, R. T., Acevedo-Arozena, A., Adeli, K., Agholme, L., Agnello, M., Agostinis, P., Aguirre-Ghiso, J. A., *et al.* (2012). Guidelines for the use and interpretation of assays for monitoring autophagy. *Autophagy* **8**, 445–544.

Kroemer, G., and Levine, B. (2008). Autophagic cell death: the story of a misnomer. *Nature Rev. Mol. Cell. Biol.* **9**, 1004–1010.

Kuma, A., Hatano, M., Matsui, M., Yamamoto, A., Nakaya, H., Yoshimori, T., Ohsumi, Y., Tokuhisa, T., and Mizushima, N. (2004). The role of autophagy during the early neonatal starvation period. *Nature* **432**, 1032–1036.

Liang, C. (2010). Negative regulation of autophagy. *Cell Death. Diff.* **17**, 1807–1815.

Liu, R., Zhi, X., and Zhong, Q. (2015). ATG14 controls SNARE-mediated autophagosome fusion with a lysosome. *Autophagy* **11**, 847–849.

Lohren, H., Blagojevic, L., Fitkau, R., Ebert, F., Schildknecht, S., Leist, M., and Schwerdtle, T. (2015). Toxicity of organic and inorganic mercury species in differentiated human neurons and human astrocytes. *J. Trace. Elem. Med. Biol.* **32**, 200–208.

Lu, T. H., Chen, C. H., Lee, M. J., Ho, T. J., Leung, Y. M., Hung, D. Z., Yen, C. C., He, T. Y., and Chen, Y. W. (2010). Methylmercury chloride induces alveolar type II epithelial cell damage through an oxidative stress-related mitochondrial cell death pathway. *Toxicol. Lett.* **194**, 70–78.

Lu, T. H., Su, C. C., Chen, Y. W., Yang, C. Y., Wu, C. C., Hung, D. Z., Chen, C. H., Cheng, P. W., Liu, S. H., and Huang, C. F. (2011). Arsenic induces pancreatic beta-cell apoptosis via the oxidative stress-regulated mitochondria-dependent and endoplasmic reticulum stress-triggered signaling pathways. *Toxicol. Lett.* **201**, 15–26.

Marino, G., Niso-Santano, M., Baehrecke, E. H., and Kroemer, G. (2014). Self-consumption: the interplay of autophagy and apoptosis. *Nature Rev. Mol. Cell. Biol.* **15**, 81–94.

Moreau, K., Renna, M., and Rubinsztein, D. C. (2013). Connections between SNAREs and autophagy. *Trends. Biochem. Sci.* **38**, 57–63.

Scorrano, L., Oakes, S. A., Opferman, J. T., Cheng, E. H., Sorcinelli, M. D., Pozzan, T., and Korsmeyer, S. J. (2003). BAX and BAK regulation of endoplasmic reticulum $Ca^{2+}$: a control point for apoptosis. *Science* **300**, 135–139.

Sumathi, T., Shobana, C., Christinal, J., and Anusha, C. (2012). Protective effect of Bacopa monniera on methyl mercury-induced oxidative stress in cerebellum of rats. *Cell. Mol. Neurobiol.* **32**, 979–987.

Tabas, I., and Ron, D. (2011). Integrating the mechanisms of apoptosis induced by endoplasmic reticulum stress. *Nat. Cell. Biol.* **13**, 184–190.

Tchounwou, P. B., Yedjou, C. G., Patlolla, A. K., and Sutton, D. J. (2012). Heavy metal toxicity and the environment. *Exs* **101**, 133–164.

Tinkov, A. A., Ajsuvakova, O. P., Skalnaya, M. G., Popova, E. V., Sinitskii, A. I., Nemereshina, O. N., Gatiatulina, E. R., Nikonorov, A. A., and Skalny, A. V. (2015). Mercury and metabolic syndrome: a review of experimental and clinical observations. *Biometals* **28**, 231–254.

Ullman, E., Fan, Y., Stawowczyk, M., Chen, H. M., Yue, Z., and Zong, W. X. (2008). Autophagy promotes necrosis in apoptosis-deficient cells in response to ER stress. *Cell. Death. Diff.* **15**, 422–425.

Vanden Berghe, T., Linkermann, A., Jouan-Lanhouet, S., Walczak, H., and Vandenabeele, P. (2014). Regulated necrosis: the expanding network of non-apoptotic cell death pathways. *Nature Rev. Mol. Cell. Biol.* **15**, 135–147.

Vergilio, C. S., Carvalho, C. E., and Melo, E. J. (2015). Mercury-induced dysfunctions in multiple organelles leading to cell death. *Toxicol. In Vitro* **29**, 63–71.

Wu, J., and Kaufman, R. J. (2006). From acute ER stress to physiological roles of the Unfolded Protein Response. *Cell. Death. Diff.* **13**, 374–384.

Zaitsu, M., Narita, S., Lambert, K. C., Grady, J. J., Estes, D. M., Curran, E. M., Brooks, E. G., Watson, C. S., Goldblum, R. M., and Midoro-Horiuti, T. (2007). Estradiol activates mast cells via a non-genomic estrogen receptor-alpha and calcium influx. *Mol. Immunol.* **44**, 1977–1985.

Zalups, R. K. (2000). Molecular interactions with mercury in the kidney. *Pharmacol. Rev.* **52**, 113–143.

Zhang, H., Wu, H., Wang, C., Xie, J., He, J., Yang, J., and Ye, J. (2014). Acute exposure to thimerosal induces antiproliferative properties, apoptosis, and autophagy activation in human Chang conjunctival cells. *Graefe's. Arch. Clin. Exp. Ophthalmol.* **252**, 275–284.

Zhang, Z., Miah, M., Culbreth, M., and Aschner, M. (2016). Autophagy in Neurodegenerative Diseases and Metal Neurotoxicity. *Neurochem. Res.* **41**, 409–422.

Zhen, Y., and Li, W. (2015). Impairment of autophagosome-lysosome fusion in the buff mutant mice with the VPS33A(D251E) mutation. *Autophagy* **11**, 1608–1622.

Zheng, Q. Y., Li, P. P., Jin, F. S., Yao, C., Zhang, G. H., Zang, T., and Ai, X. (2013). Ursolic acid induces ER stress response to activate ASK1-JNK signaling and induce apoptosis in human bladder cancer T24 cells. *Cell. Signal.* **25**, 206–213.